Scientia Iranica, Vol. 8, No. 2, pp 130–137

SCIENTIA
IRANICA

The Propagation of Turbulent Density Currents on Sloping Beds

B. Farhanieh[1], B. Firoozabadi* and M. Rad[1]

In this paper, the motion of density currents, released on sloping beds and under still bodies of clear water, is numerically investigated. The turbulent flow equations of mass, momentum and diffusion are solved simultaneously in the fixed Cartesian directions, on a non-staggered grid using finite-volume scheme. The velocity-pressure coupling is handled by SIMPLEC method. A modified $k-\varepsilon$ model is used to account for the influence of Reynolds stresses in the turbulent momentum equations. Density currents with uniform velocity and concentration enter the channel via a sluice gate into a lighter ambient fluid and move forward down the slope. Comparison of the computed velocity, concentration profiles and height of density current with the experimental data, illustrates a good agreement. The overall Richardson number reaches a constant value after a short distance from the channel inlet. In this paper, the effects of variation of concentration and flow rates in the form of Richardson or densimetric Frude and Reynolds numbers are investigated for different slopes. Concentration and velocity profiles are obtained and show a complex flow pattern which provides a physical understanding of the governing phenomena.

INTRODUCTION

Density current is formed when a fluid heavier than ambient fluid flows down an inclined bed. These flows, which are common phenomena in nature, can be produced by salinity or temperature differences and are referred to as inclined plumes or under-flows. Examples in the atmosphere include downhill motion of air cooled by flowing over snow or cold ground, advancement of a cold front under warmer air, thunderstorm outflows, snow avalanches and mud slides [1]. In the ocean, density currents are driven by salinity and temperature inhomogeneities, or as turbidity currents whose density drives are from suspended particles of silt and clay. Within the field of hydraulic engineering, examples include reservoir under and inner flows, solid driven currents in sedimentation basin and treatment plants, buoyant effluent discharges, advancement of salt water under fresh water in estuaries and when a lock gate is opened at a mouth of a river. Turbid density currents are an important mechanism for the transport of sediment from continental rim to the abyssal plain in oceans [2]. They are the subject of a great number of studies by investigators. Driven by density differences between the sediment laden inflow and the clear water in the reservoir, the density current plunges between the clear water and moves toward the dam as a submerged current. Only a few direct observations of density currents in the field have been made [3]. Field measurements are rendered difficult by the need to work under water, the substantial equipment requirements and the tendency of swift currents to destroy measuring apparatus [4].

Density currents have been observed not only in reservoirs of the Yellow River and Sanmenxia, in which the yearly mean sediment concentration is tens of kilograms per cubic meter, but also in reservoirs of rivers with low sediment conditions. The sediment concentration in these typical rivers is about 1-2 kg/m^3 [5]. Bottom outlets may be used to vent density currents, in some cases more than half of the inflowing sediment load.

The density current consists of a head with a complex three-dimensional flow structure at the leading edge, followed by a thinner flow. This leading edge is commonly referred to as a "front part" and the upstream is termed the "body part". The propagation of a front at a bottom is influenced by real-

1. *Department of Mechanical Engineering, Sharif University of Technology, Tehran, I.R. Iran.*
*. *Corresponding Author, Department of Mechanical Engineering, Sharif University of Technology, Tehran, I.R. Iran.*

fluid effects so that its analysis requires a realistic approach. The no-slip condition causes the frontal stagnation point to rise above the bottom and the front speed, relative to the ambient velocity, decreases as this velocity increases [6]. In a density current flowing horizontally, the head remains quasi-steady and is about twice as deep as the following flow [7], but in current flowing down a slope, the size of the head continuously increases. A "universal profile" of a density current head does not exist and is strongly modified by opposing and following ambient flow and other physical effects. As the flow velocity and, hence, the Reynolds number of the flow increase, the shape of the density current changes and intense motion and mixing occur. The dynamics of a density current was analyzed first by Von Karmen (1940) and later by BenJamin [8]. Turner [9] has analyzed one-dimensional density current for the laminar and turbulent flows. Numerical investigation of turbulent density current for different modes and particle-laden flows has been undertaken by Akiyama and Stefan [9-12]. These authors assumed jet velocity distribution in turbulent model and solved the equations of turbidity current. For integral solution of equations, Akiyama assumed the thickness of the deposit to be 5% of the current depth and then performed the integration from the bed up to the interface. Through knowing the boundary condition at the bed and assuming values for several variables at the interface, he managed to compute the depth, buoyancy flux, Richardson number and the non-dimensional average velocity in the flow direction. The results of his numerical integration have been compared with the emperical results and it has been shown that the overall Richardson number, after a short distance from the channel inlet, reaches a constant value. This result agrees well with the assumption made by Turner [9] who solved the equations for a stabilized case.

Differential solutions for the equations of density current have been performed for special cases. Bonnecaze et al. [13] have solved the particle driven density current equations as shallow water equations for two cases of unsteady, one-dimensional, uniform velocity and concentration on a flat plate. This solution has been conducted for single-layer flow (a case where the height of density current is very small compared to the height of clear water) and two-layer flow. In the solution of the equations, assumptions such as no entrainment and the negligibility of viscosity have been considered. Bonnecaze solved the equations using the two step Lax-Wendroff scheme [13]. The resulting solution is consistent with emperical results in terms of shape and appearence of particle density current front. Parker et al. [14] have combined the equations of mass and momentum conservations with the inflow equation of the bed matter and solved them numerically. Stacey and Bowen [15] solved the equations of turbidity current for unsteady, turbulent and one-dimensional cases by neglecting the inertial terms and, thereby, obtaining the effect of particle fall velocity in the distribution of flow velocity, concentration and depth of current. Ostraka and Anderson [16] have compared the various methods of solution for turbulent density currents. They verified these methods under identical conditions. Although they were able to demonstrate the weak and strong points of the numerical methods used in the solution of unsteady density currents, it has little applicablility for solving equations of particle driven density currents.

In the present work, a complete two-dimensional numerical model is developed to simulate the motion of a density current. The results are compared with the reported laboratory experimental data.

GOVERNING EQUATIONS

In this paper, the analysis of the steady state equations for predicting the behavior of the body of density current is considered. Figure 1 shows the definition sketch of the density current under investigation.

The turbulent equations are given for two dimensions, based on boundary-layer and Boussinesq approximations, as follows:

- Continuity equation:

$$\frac{\partial U_i}{\partial x_i} = 0, \tag{1}$$

- Momentum equation

$$U_j \frac{\partial U_i}{\partial x_j} = -(1/\rho)\frac{\partial P}{\partial x_i} + g_i' + \frac{\partial}{\partial x_j}(\nu + \nu_t \frac{\partial U_i}{\partial x_j}). \tag{2}$$

Considering Boussinesq approximation, the effects of density difference are neglected in the treatment of the inertial terms but included in the buoyancy force term. The last term in Equation 2 results from the basic $k-\varepsilon$ model relationship between turbulent stress and mean velocity gradient. The turbulent viscosity being evaluated from $\nu_t = C_\mu k^2/\varepsilon$. k and ε are treated as transported scalers with appropriate source and sink terms as:

- Turbulence kinematic energy per unit mass,

$$U_j \frac{\partial k}{\partial x_j} = \frac{\partial}{\partial x_j}\left((\nu + \frac{\nu_t}{\sigma_k})\frac{\partial k}{\partial x_j}\right) + P_k - \varepsilon, \tag{3}$$

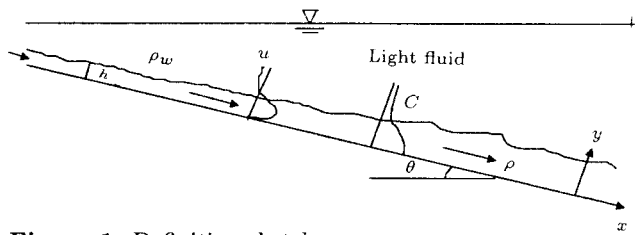

Figure 1. Definition sketch.

- Dissipation rate of turbulence energy,

$$U_j \frac{\partial \varepsilon}{\partial x_j} = \frac{\partial}{\partial x_j}\left((\nu + \frac{\nu_t}{\sigma_\varepsilon})\frac{\partial \varepsilon}{\partial x_j}\right) + C_1 \frac{\varepsilon}{k} P_k - C_2 \varepsilon^2/k, \tag{4}$$

where the production term P_k, due to velocity gradients, has the following form,

$$P_k = \nu_t \left(\frac{\partial U_i}{\partial x_j} + \frac{\partial U_j}{\partial x_i}\right)\frac{\partial U_i}{\partial x_j}. \tag{5}$$

The standard value of constants in the above equations were assumed as [17]:

C_μ	C_1	C_2	σ_k	σ_ε
0.09	1.44	1.92	1.0	1.3

Because of the $k-\varepsilon$ model weakness in the near wall region, in this analysis, constants are modified according to low Reynolds number models [18], to predict the near-wall turbulence in the density current. The modifications of constants are as follows:

$$f_\mu = \exp\left(-3.5/(1+\frac{R_t}{50})^2\right), \tag{6}$$

$$f_2 = 1 - 0.3\exp(-R_t)^2, \tag{7}$$

where,

$$R_t = \frac{k^2}{\varepsilon\nu}, \tag{8}$$

and then $C_\mu = C_\mu \times f_\mu$, $C_2 = C_2 \times f_2$.

It is necessary to predict the concentration of salt in the flow in order to estimate the amount of the material. The governing equation for the concentration is presented by:

$$U_j \frac{\partial C}{\partial x_j} = \frac{\partial}{\partial x_j}\left(\lambda + \varepsilon_s \frac{\partial C}{\partial x_j}\right). \tag{9}$$

The mean concentration C is defined at the center point of control volume and Equation 9 is solved simultaneously with the fluid flow equations. The turbulent diffusivity ε_s can be expressed in terms of turbulent Schmidt number Sc as:

$$\varepsilon_s = \frac{\nu_t}{Sc}. \tag{10}$$

While the Schmidt number, similar to the turbulent Prandtl number, is expected to be affected by the buoyancy which is assumed to be unity here [17].

BOUNDARY CONDITIONS

Boundary conditions at the inlet are known and similar to the experimental models where salt-solution flow with uniform velocity and concentration enters the channel under the still bodies of water via a sluice gate onto a surface inclined at angle θ . Inlet k and ε boundaries are used here,

$$k_{in} = (I \times U_{in})^2, \tag{11a}$$

$$\varepsilon_{in} = C_\mu^{3/4}\, k_{in}^{3/2}/(\alpha \times b), \tag{11b}$$

where I is the relative turbulent intensity with a measured value in this investigation of about 0.1, $C_\mu = 0.09$, the factor $\alpha = 0.1$ and b is the gate opening height.

A fully developed condition is prescribed at the outlet of the channel. Because of the higher depth of the surrounding water compared with the depth of the density current, the upper boundary is considered symmetrical. Thus, there is no flux of any kind normal to the upper boundary, either convective or diffusive. The normal velocity component, as well as the normal gradient of the remaining dependent veriables, are zero. On the bed, due to the application of low Reynolds turbulence model, no slip conditions, i.e. $u = v = k = \varepsilon = 0.0$, are used in connection with the wall boundaries and the concentration gradient is set to zero.

SOLUTION PROCEDURE

The governing equations are solved by a finite-volume method using boundary fitted coordinates. The momentum, diffusion, turbulent kinetic enegy and dissipation equations are solved for the velocity components and concentration u, v, C, k, and ε in the fixed Cartesian directions on a non-staggered grid. All the variables are, thus, stored at the center of the control volume. The velocity components at the control volume faces are computed using Rhie-Chow interpolation method [19] and the pressure-velocity coupling is handled by SIMPLEC method [20]. The convective terms are treated through the hybrid scheme. TDMA-based algorithms are applied for solving the algebraic equations. Further details are provided by Davidson and Farhanieh [21]. The solution procedure is iterative and the computations are terminated when the sum of absolute residuals, normalized by the inflow fluxes, were below 10^{-5} for all the variables. To achieve convergence of the solution, under-relaxation factor of 0.5 was chosen for all the variables. Depending on velocity and slope, around 3000-5000 iterations are required to achieve convergence in the velocity fields. However, for concentration, turbulent energy and dissipation fields, convergence is much quicker.

The mesh points are chosen as uniform in the flow direction but, in the normal direction, the grid points are distributed in a non-uniform manner with a higher concentration of grids close to the bed surface. Each control volume contains one node at its center but the boundary adjacent volumes contain two nodes. The effects of different mesh size on flow progression and velocity profiles were obtained, no changes in the results can be observed by increasing the mesh size beyond 172×42. Thus, the mesh size 152×42 is chosen for performing the computation.

RESULTS AND DISCUSSION

The experimental data presented in Table 1 show the flow conditions which have been used as input data in the computer program.

Figure 2 illustrates a comparison between measured and computed streamwise velocity at two different locations. The maximum velocities are underpredicted, whereas the overall shapes of the profiles are in good agreement with the measured values. However, the numerical viscosity affects the magnitude and location of maximum velocity.

The depth $h(x)$ together with the average velocity and concentration $\bar{u}(x)$ and $\bar{c}(x)$ of a density current are expressed as [15]:

$$\bar{u}(x)h(x) = \int_o^\infty u(x,y)dy, \tag{12}$$

$$\bar{u}(x)^2 h(x) = \int_o^\infty u(x,y)^2 dy, \tag{13}$$

$$\bar{c}(x)h(x) = \int_o^\infty c(x,y)dy, \tag{14}$$

$$Ri(x) = \frac{g'(x)h(x)\cos(\theta)}{\bar{u}(x)^2}, \tag{15}$$

$$g'(x) = g\bar{c}(x)(\rho_s - \rho_w)/\rho_w, \tag{16}$$

where $Ri(x)$ is the bulk Richardson number at each x station. A comparison of the measured depth of density current with the predictions is presented in Figure 3. As can be seen from this figure, the predicted depths are in good agreement with Akiyama experiments [12]. It can also be seen from Figure 3 that at higher bed slopes, the driving force increases and the depth of the current decreases.

The calculated averaged-layer properties (Equations 12-16) of run no. 2 are presented in Figure 4. Due to the entrainment of upper lighter fluid and density current at the interface, the current depth

Table 1. Inlet conditions.

Run no.	Ref	Uin (cm/s)	hi (cm)	Slope (%)	Cin (%)	Ri_o	Re_o
1	[4]	11.0	3.0	8.0	2.5	0.29	3340
2	[12]	6.84	5.0	10.0	1.0	0.57	3438
3	[12]	6.30	4.0	14.0	1.2	0.73	2538
4	[22]	11.0	2.0	1.0	1.2	0.11	2215
5	[22]	11.0	2.0	2.5	0.63	0.11	2215
6	[22]	11.0	2.0	2.5	1.2	0.11	2208
7	[22]	8.0	2.0	2.5	1.2	0.22	1611

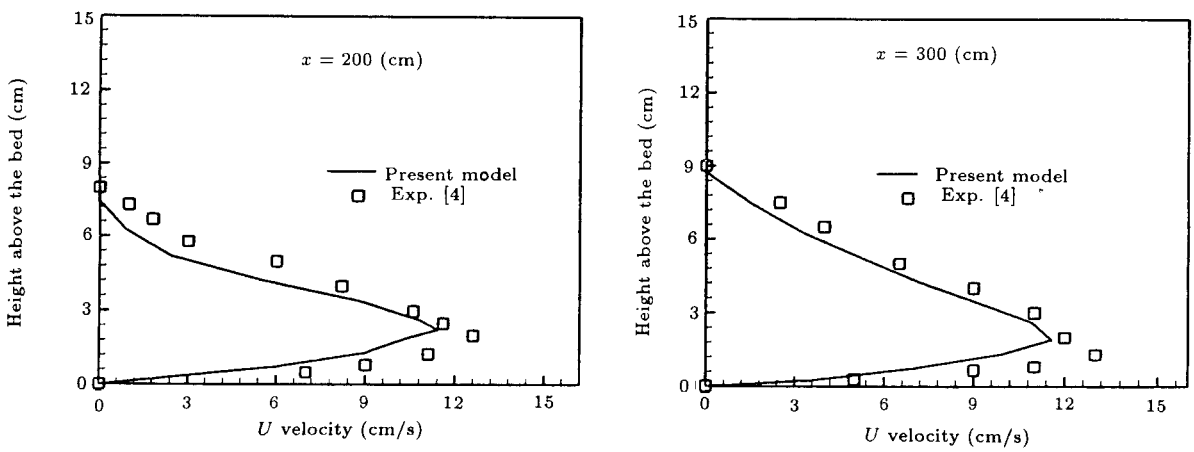

Figure 2. Comparison of the calculated velocity profiles with Garcia experiments [4].

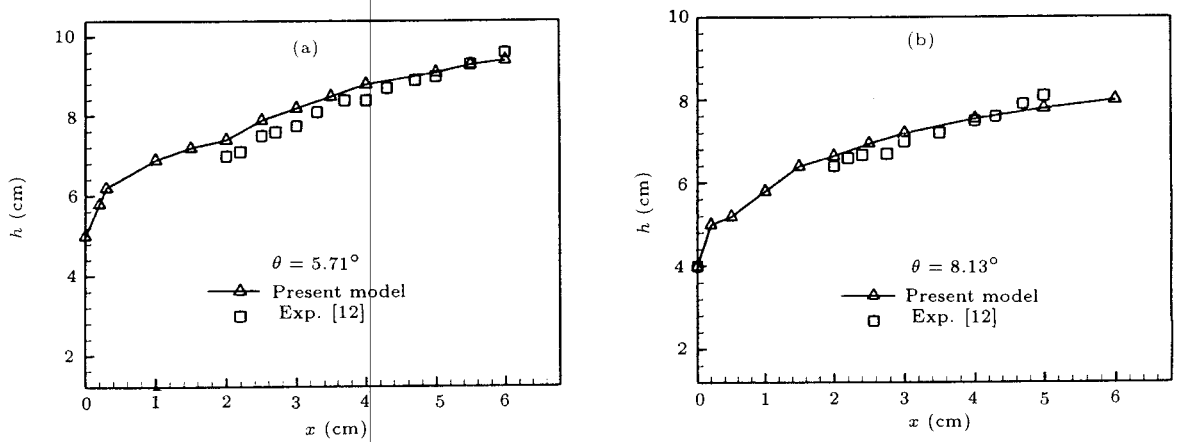

Figure 3. The depth of the density current compared with Akiyama data [12]. (a) Run no. 2 and (b) Run no. 3.

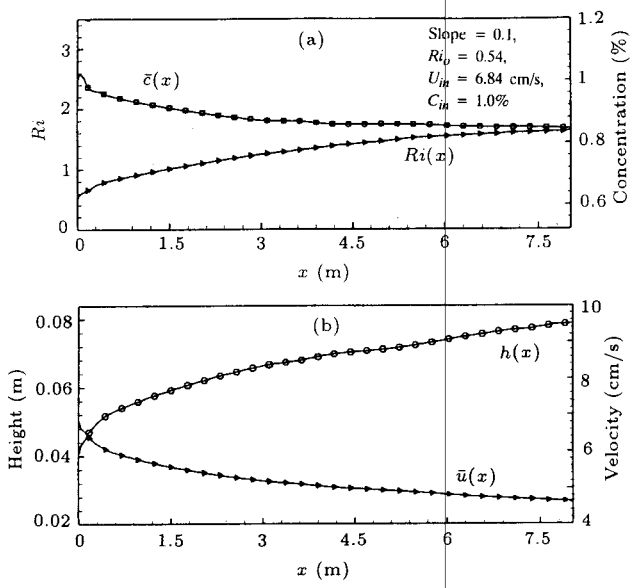

Figure 4. Calculated averaged-layer properties of run no. 2.

h increases in x direction and the averaged velocity and concentration decrease. The overall Richardson number, after a distance from the inlet, reaches a constant value, called "establishment flow". It can be observed from Figure 4 that Richardson number varies slightly after 3 meters, which is consistent with the results of Turner [9], Akiyama [10] and Alavian [1].

Figure 5 shows the effect of inlet velocity on the depth of density current. This figure also demonstrates the comparison of numerical depth with the experimental data of Rad et al. [22] which are in good agreement. It can be seen from Figure 5 that the depth of density current increases while inlet velocity decreases.

The effects of bed slope and inlet concentration on depth have been shown in Figure 6. Increasing the bed slope from 1.0% to 2.5% does not affect the inlet flow regime, while by increasing the streamwise driving force, the averaged- layer velocity increases and, hence,

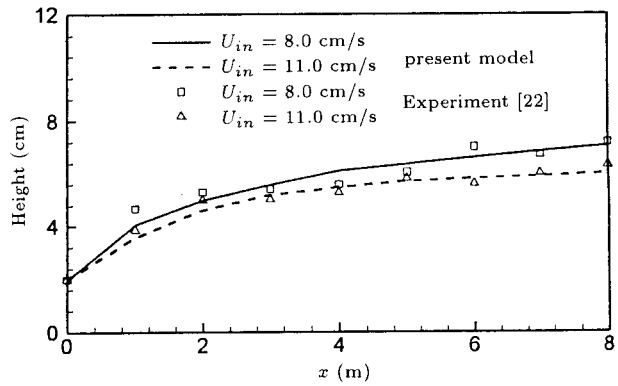

Figure 5. The effect of entrance velocity on the depth of density current and comparison with experimental data [22], run nos. 6 and 7.

as can be seen from Figure 6a, the depth of the current decreases. The flow regime may be changed as the inlet concentration has an intense effect on Richardson number. Increasing the inlet concentration, in the range of run nos. 5 and 6, decreases the depth of the current.

Figure 7 depicts the contour lines of concentration, streamwise velocity and velocity vectors of run no. 1. Diffusion of momentum in a normal direction is more than concentration diffusion and density current can move upper fluid up to a higher height above the bed, as can be observed from Figure 7a. Velocity contour lines have been shown in Figure 7b. Due to the high slope of the bed, the inlet velocity (11.0 cm/s), along the motion of density current on the bed, becomes up to 12.5 cm/s. The maximum velocity contour line lies nearly in the middle part of the current depth. In each x station and above the velocity profiles, a few negative velocity vectors can be seen, which are caused by the entrainment. The conservative density current and entrainment region can be observed from Figure 7.

Figure 8 shows the streamwise velocity and concentration profiles of run no. 2 at different locations.

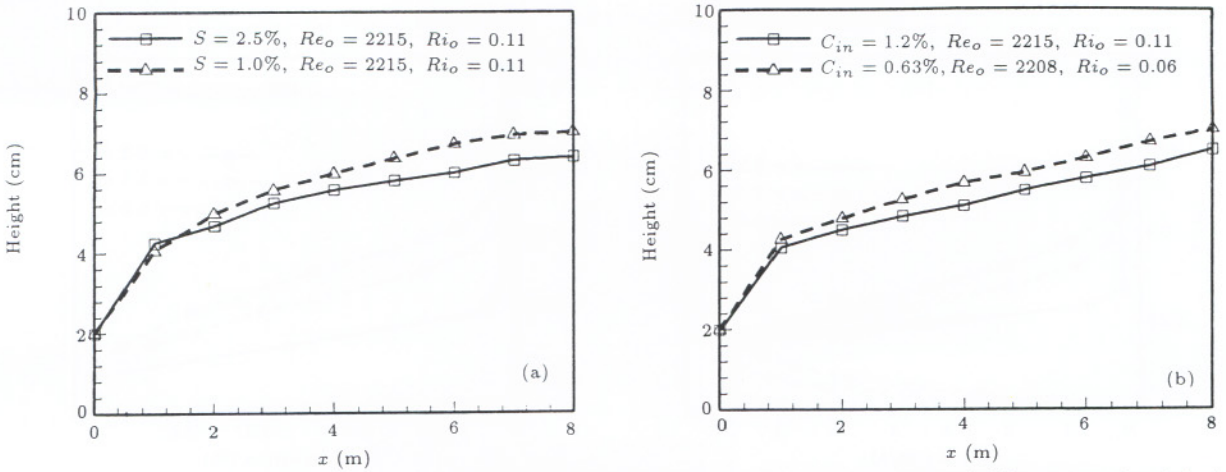

Figure 6. The effects of bed slope and inlet concentration on the depth of density current. (a) Run nos. 4 and 5, (b) Run nos. 5 and 6.

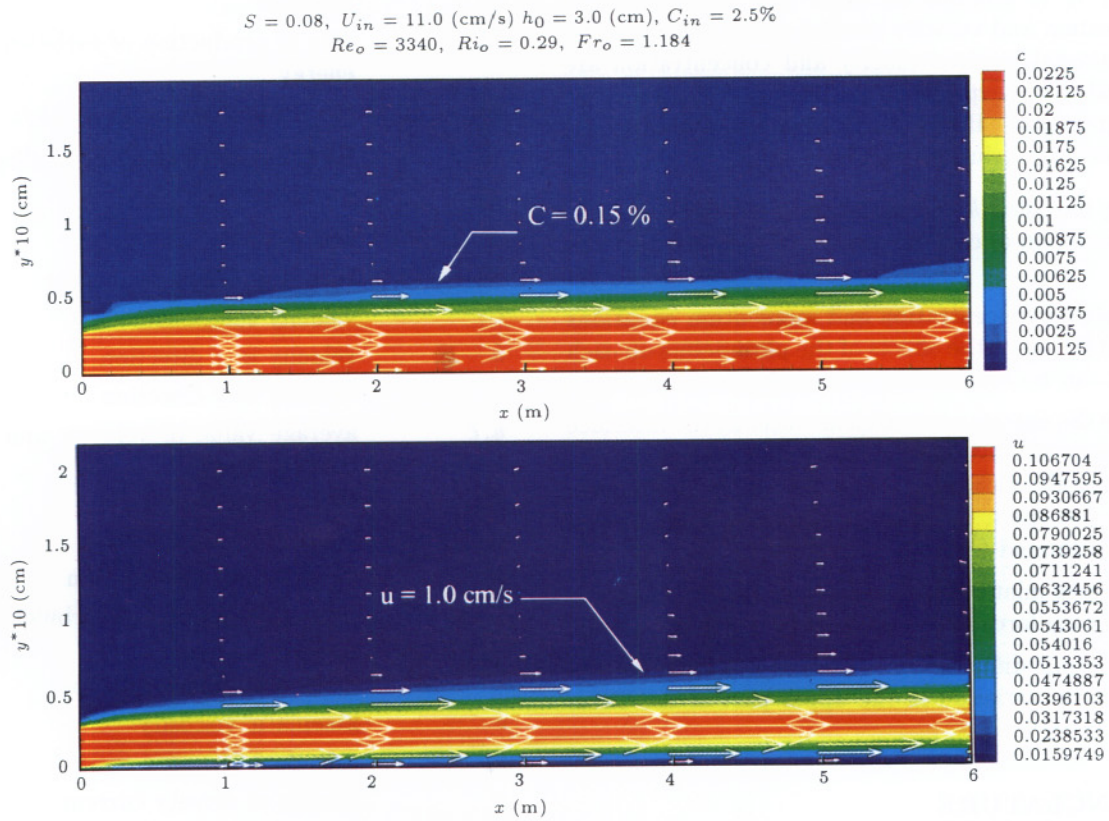

Figure 7. Contour lines of concentration and streamwise velocity and their velocity vectors of run no. 1.

A uniform velocity is introduced at the inlet, which is 5.0 cm high. The uniformity of the velocity profile is preserved even at $x = 0.2$ m. However, the velocity profile becomes fully developed at $x = 6.0$ m and the diffusion depth at this point reaches a height of 12.0 cm. Figure 8b presents the entrainment distance versus the conservative density current. At $x = 0.2$ m, the entrainment distance is 2.0 cm whereas at $x = 6.0$ m, this distance increases to 5.0 cm. The depth of density current and its variation can also be observed in Figure 8b.

CONCLUSION

The equations of turbulent density current are solved by SIMPLEC method. A modified $k - \varepsilon$ model was used to account for the influence of Reynolds stresses in the turbulent momentum equations. Using the

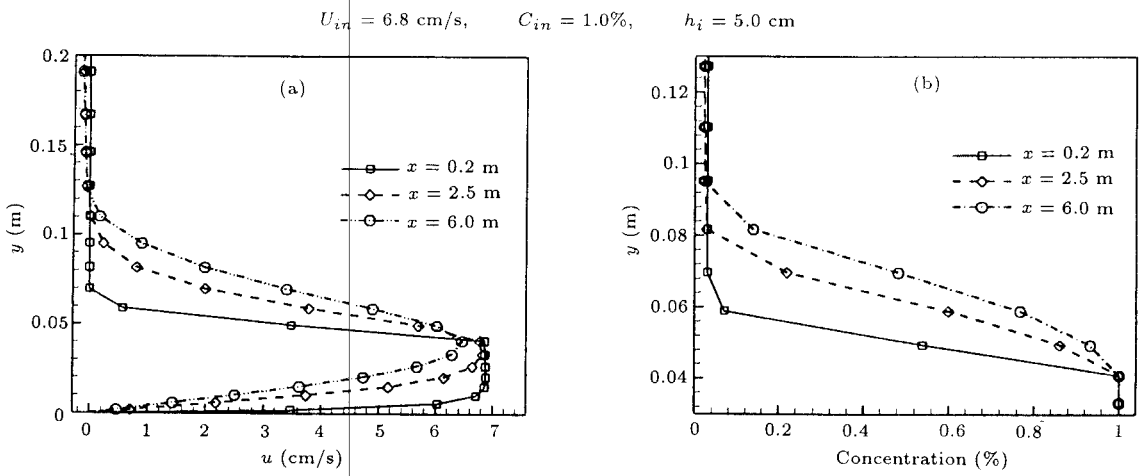

Figure 8. Velocity and concentration profiles at different locations of run no. 2.

solution, it is possible to show the distribution of concentration and velocity profiles of the current. The computational height, velocity and concentration are compared with experimental data and demonstrate good agreement. Based on the results of this study, the following conclusions can be drawn:

1. Using modified $k-\varepsilon$ model, it is possible to show the variation of concentration and velocity near the bed.
2. By solving concentration and momentum equations simultaneously, the effects of the parameters on each other can be considered.
3. While the entrainment of clear water at the interface decreases the averaged velocity and concentration, the overall Richardson number, after a distance from the inlet, reaches a constant value called "establishment flow".
4. Increasing inlet concentration and velocity increases the driving force and decreases the depth of current.
5. Momentum diffusion in a normal direction results in velocity variation in the upper part of the dense layer.

NOMENCLATURE

b	height of sluice gate
C	concentration, $C = (\rho - \rho_w)/(\rho_s - \rho_w)$
C_1, C_2, C_μ	standard constants of $k-\varepsilon$ model
Fr	densimetric Frude number, $Fr = u/\sqrt{g'h\cos\theta}$
g	gravitational acceleration
g'	reduced gravitational acceleration, $g' = g(\rho - \rho_w)/\rho_w$
h	density current depth
k	turbulent kinetic energy
P	pressure
P_k	rate of production of turbulent kinetic energy
Re	Reynolds number, $Re = uh/\nu$
Ri	Richardson number, $Ri = g'h\cos\theta/u^2$
Rt	$k^2/\varepsilon\nu$
S	bed slope
Sc	turbulent Schmidt number
U_i	velocity components
u	velocity in x direction
v	velocity in y direction
$\bar{u}, \bar{c}$	average value of velocity and concentration
x	streamwise coordinate
y	transversal coordinate
α	factor of inlet dissipation
ε	rate of dissipation of turbulent kinetic energy
λ	molecular diffusion factor
ν	kinematic viscosity
ν_t	turbulent viscosity
ρ	density of density current
ρ_w	water density
ρ_s	salt density
θ	angle of the bed
$\sigma_k, \sigma_\varepsilon$	turbulent constants of $k-\varepsilon$ model

REFERENCES

1. Alavian, V. "Behavior of density currents on an incline", *J. of Hydraulic Eng., ASCE*, **112**(1) (1986).
2. Liu, Q., Schalpfer, D. and Buhler, J. "Motion of dense thermal on incline", *J. of Hydraulic Eng.*, **117**(12) (1991).

3. Chikita, K. and Okumura, Y. "Dynamics of turbidity currents measured in Katsurasawa reservoir, Hokkido, Japan", *J. of Hydrology*, **117** (1990).
4. Garcia, M. "Depositional turbidity currents laden with poorly sorted sediment", *J. of Hydraulic Eng., ASCE*, **120**(11) (1994).
5. Fan, J. and Morris, G.L. "Reservoir sedimentation. I-delta and density current deposition", *J. of Hydraulic Eng., ASCE*, **118** (1992).
6. Kranenburge, C. "Gravity-current fronts advancing into horizontal ambient flow", *J. of Hydraulic Eng.*, **119**(3) (1993).
7. Simpson, J.E. "Gravity current in the laboratory, atmosphere and ocean", *Ann. Rev. Fluid Mech.*, **14** (1982).
8. Benjamin, T.B. "Gravity currents and related phenomena", *J. Fluid Mech.*, **31** (1968).
9. Turner, J.S., *Buoyancy Effects in Fluids*, Cambridge University Press, London, U.K. (1973).
10. Akiyama, J. and Stefan, H.G. "Turbidity current with erosion and deposition", *J. of Hydraulic Eng., ASCE*, **111**(12) (1985).
11. Akiyama, J. and Stefan, H.G. "Turbidity current simulation in a diverging Channel", *Water Resources Resarch*, **24**(4) (1988).
12. Akiyama, J., Ura, M. and Wang, W. "Physical-based numerical model of inclined starting plumes", *J. Hydraulic Eng., ASCE*, **120**(10) (1994).
13. Bonnecaze, R.T., Huppert, H.E. and Lister, J.R. "Particle driven gravity currents", *J. Fluid Mech.*, **250** (1993).
14. Parker, G., Fukushima, Y. and Pantin, H.M. "Self - accelerating turbidity currents", *J. Fluid Mech.*, **171** (1986).
15. Stacey, M.W. and Bowen, A.J. "The vertical structure of turbidity currents and a necessary condition for self-maintenance", *J. Geophisical Research*, **93**(c4) (1988).
16. Straka, J.M. and Anderson, J.R. "Numerical solution of a non-linear density current: A benchmark solution and comparisons", *Int. J. for Numerical Methods in Fluids*, **17**, pp 1-22 (1993).
17. Lyn, D.A., Stamou, A.I. and Rodi, W. "Density currents and shear-induced fluctuation in sedimentation tanks", *J. of Hydraulic Eng.*, **118**(6) (1992).
18. Karimipanah, T. "Turbulent jets in confined spaces-application in mixing ventilation experimental and numerical studies", PhD Thesis, Royal Institute of Technology, Gavle, Sweden (1996).
19. Farhanieh, B. and Sunden, B. "Laminar heat transfer and fluid flow in streamwise-periodic corrugated square ducts for compact heat exchangers", **HTD-V.201**, Compact Heat Exchangers for Power and Process Industries, Shah, R.K. et al., Eds., ASTM Book no. H00759 (1992).
20. Patankar, S.V., *Numerical Heat Transfer and Fluid Flow*, McGraw-Hill, Washington (1980).
21. Davidson, L. and Farhanieh, B., *A Finite Volume Code Employing Collocated Variable Arrangement and Cartesian Velocity Components for Computation of Fluid Flow and Heat Transfer Complex Three- Dimensional Geometries*, Cahlmers University of Technology, Goteborg, Sweden (1991).
22. Rad, M. and Firoozabadi, B. "Confined turbidity current and its application in reservoirs", *Int. Conf. Civil Engineering*, Sharif University of Technology, Tehran, I.R. Iran (1997).